Influence of the $N=50$ shell closure on mean square charge radii of strontium

F. Buchinger, R. Corriveau, and E. B. Ramsay
Foster Radiation Laboratory, McGill University, Montreal, Quebec, Canada H3A 2B2

D. Berdichevsky and D. W. L. Sprung
Physics Department, McMaster University, Hamilton, Ontario, Canada L8S 4M1

(Received 28 May 1985)

Isotope shifts of the stable strontium isotopes ^{84}Sr, ^{86}Sr, ^{87}Sr, and ^{88}Sr and the radioactive isotopes ^{89}Sr and ^{90}Sr have been measured using laser spectroscopy on collimated atomic beams. The changes in mean square charge radii extracted from the isotope shifts show a pronounced shell effect at the closed neutron shell $N=50$. The experimental data are compared with the predictions of the droplet model and Hartree-Fock plus BCS calculations. The analysis suggests that the changes in mean square charge radii are due to a change in size, a change in the predominantly dynamic deformation, and a change in the diffuseness of the nuclear charge distribution.

I. INTRODUCTION

Accurate optical isotope shift measurements based on laser spectroscopy experiments provide systematic information on changes in mean square radii as a function of neutron number.[1]

An interpretation of the changes in mean square charge radii in a model-dependent way allows one to extract information about nuclear structure. Particularly, changes in nuclear deformation, as a function of neutron number, are commonly derived in a two-parameter model[2] by uniquely relating the changes in mean square charge radii to a change of size and deformation of the nuclear charge distribution. By relying originally on the liquid drop model and later on the droplet model[3] for the description of the rearrangement of the nuclear charge distribution with neutron number, this two-parameter approach was used successfully to explain the overall behavior of changes in nuclear charge radii in long isotopic series of many elements.[4]

Still, there remained cases which indicated the shortcomings of this approach. An extension of the two-parameter model by adding a third term related to the change in skin thickness of the nuclear charge distribution has been discussed in connection with isotope shift measurements in krypton[5] and cadmium.[6] In both cases, the authors associate the changes in the skin thickness with a neutron shell or subshell closure, indicating that shell effects are not solely expressed through their influence on nuclear deformation.

The subject of changes in diffuseness with isotope and their influence on changes in mean square charge radii has also received recent interest from the theoretical side.[7] In a comparison between droplet model (DM) and Hartree-Fock (HF) predictions for changes in mean square charge radii, the droplet model has been criticized for its too schematic treatment of the surface diffuseness, and thus its utility for the interpretation of the experimental data has been questioned.

As a contribution to this discussion, and in order to study the influence of changes in surface thickness in more detail, we have investigated changes in mean square charge radii in a series of strontium isotopes near the closed neutron shell at $N=50$.

The experiment, consisting of isotope shift measurements using laser spectroscopy on collimated atomic beams, is described in Sec. II. We have evaluated changes in mean square charge radii for the series of investigated isotopes (Sec. III) and discussed the experimental data in the framework of the droplet model with special emphasis on the effects of changes in nuclear diffuseness on the charge radii (Sec. IV A). We have, furthermore, calculated the changes in mean square charge radii of the investigated even isotopes by means of the HF plus BCS method using the effective forces SKa (Ref. 8) and G0P (Ref. 9). In Sec. IV B, the droplet model and HF predictions for the changes in mean square charge radii are compared and a leptodermous interpretation of the HF results is given.

II. EXPERIMENTAL METHOD

The isotope shift (IS) in strontium (Sr) was measured using dye-laser-induced fluorescence on a highly collimated atomic beam. We have investigated the stable isotopes ^{84,86,87,88}Sr in the SrI $5s^2\ ^1S_0-5s5p\ ^1P_1$ ($\lambda=460.7$ nm) and $5s^2\ ^1S_0-5s5p\ ^3P_1$ ($\lambda=689.3$ nm) transitions. In addition, the IS of the radioactive isotopes ^{89}Sr ($T_{1/2}=50.5$ *d*) and ^{90}Sr ($T_{1/2}=29$ yr) were measured in the blue line.

A. Apparatus

A schematic view of the apparatus used for the IS measurements in Sr is shown in Fig. 1.

The isotope under investigation was evaporated from an atomic beam oven. The oven consists of a directly heated carbon cylinder which contains a tantalum crucible. The crucible is electrically insulated from the carbon piece so that the carbon mantle acts as an indirect heater for the crucible. The atomic beam evaporates through two 0.5

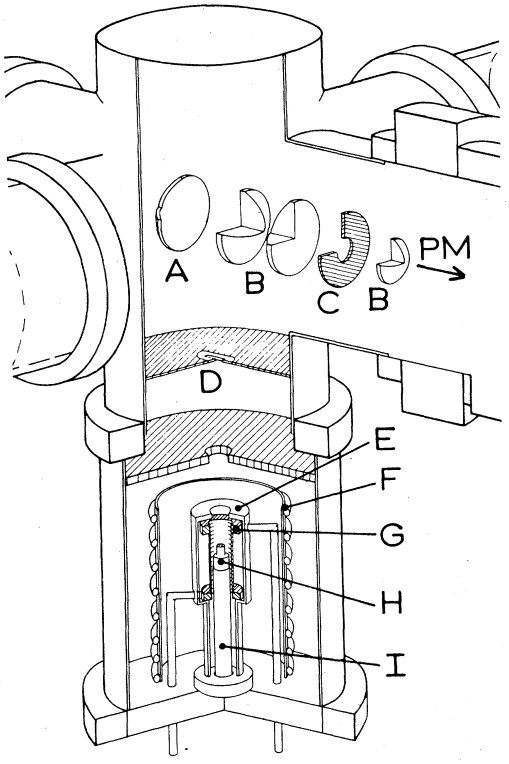

FIG. 1. Schematic view of the atomic beam apparatus. A: spherical mirror; B: lens; C: spatial hole filter; D: collimation slit; E: heat shield; F: water-cooled heat shield; G: graphite oven; H: crucible; I: crucible support; PM: photomultiplier.

mm wide and 8 mm long channels in the top of the crucible. The oven is surrounded by a boron nitride heat shield and a water-cooled copper mantle. Temperatures up to 1400 °C are obtained with this heating arrangement. The evaporated beam is collimated by a set of apertures (collimation ratio 4×10^{-3}) and is excited by laser light incident at right angles in an interaction region 15 cm away from the oven.

Our laser system consists of a ring dye laser pumped by an Ar^+ laser. Light with $\lambda=460.7$ nm for the excitation of the SrI $5s^2\ ^1S_0-5s\,5p\ ^1P_1$ transition is generated by running the dye laser with Stilben 3. A single mode output power of 25 mW is achieved when the dye laser is pumped with 2 W uv light from the Ar^+ laser. For spectroscopy in the $5s^2\ ^1S_0-5s\,5p\ ^3P_1$ ($\lambda=689.3$ nm) transition, a single mode output power of 200 mW is obtained, using the DCM dye pumped by the 514 nm line of the Ar^+ laser at 6 W.

The fluorescence light from the laser excited atoms is collected using a spherical mirror and imaged by a lens system, which includes a spatial hole filter, onto the photocathode of a photomultiplier tube (RCA 8850, RCA C31034). The detection efficiency of the system is on the order of 1%. This is determined by the solid angle covered (25% of 4π), the reflectivity of the optical components (4% per surface), the transmission of an interference filter used to suppress background from oven light, and the quantum efficiency of the photomultiplier ($\sim15\%$). Background from scattered laser light is minimized by positioning, at the Brewster angle, the entrance and exit windows for the laser beam on side arms of the apparatus 85 cm away from the interaction region and by introducing in each arm a set of knife-edged conic apertures. The counting rate from scattered laser light is typically 5×10^3 counts per sec per mW laser power. The contribution of the oven light to the background is roughly 10^3 counts per sec at maximum temperature.

The data acquisition system consists of a photon counting setup interfaced through CAMAC to an IBM personal computer. The computer also controls the laser scan and registers the signal from a Fabry Perot etalon which is used in order to establish a frequency scale. The free spectral range of the etalon is determined to be FSR = 151.8(3) MHz from the precisely known hyperfine structure splitting of the ^{133}Cs ground state measured in the CsI $6s\ ^2S_{1/2}-7p\ ^2P_{1/2}$ ($\lambda=455.5$ nm) transition.[10]

B. Preparation of the probe

The IS of the stable Sr isotopes was investigated using naturally abundant metallic Sr. The radioactive ^{89}Sr and ^{90}Sr are commercially available in the form of $SrCl_2$ and $Sr(NO_3)_2$ in acid solution. Both isotopes are fission produced and the production of light isotopes is strongly suppressed due to their lower fission yields. The samples were used without further mass separation. Using an aged probe of ^{90}Sr yields, as the only contamination, ^{88}Sr, whereas a freshly produced Sr probe for the measurement of ^{89}Sr contained contaminations from both the ^{88}Sr and ^{90}Sr.

For the IS measurements the Sr compounds were transferred into the crucible and the solvent was evaporated. For the formation of an atomic beam, the Sr compounds were reduced without using a catalyst since the strong contamination by stable Sr isotopes, present in catalysts such as calcium or aluminum, masks the signal from the weak radioactive isotopes. However, by heating the Ta crucible to 800 °C for $SrCl_2$ and 1100 °C for $Sr(NO_3)_2$, atomic Sr beams can be obtained with sufficient intensities for laser spectroscopy studies ($I\gtrsim10^6$ atoms $\sec^{-1}$). Tests with stable Sr compounds show that no lines from Sr molecules are present in the frequency region of interest. The total amount of Sr transferred into the crucible was 5×10^{15} atoms for ^{90}Sr and 2×10^{13} atoms for ^{89}Sr. Measurements in ^{89}Sr were carried out for longer than 3 h and did not exhaust the sample.

C. Measurements and data analysis

The atomic beam was excited by linearly polarized laser light. Measurements on the ^{89}Sr sample were carried out using light polarized perpendicular ($\theta=90°$) and parallel ($\theta=0°$) with respect to the axis of observation. The different angular distributions of the emitted fluorescence light for the contaminating even isotopes ^{88}Sr and ^{90}Sr ($I=0$, intensity $\propto\sin^2\theta$) and the odd isotope ($I=\frac{5}{2}$, intensity $\propto1+\cos^2\theta$) allows an enhancement of the signal

of ^{89}Sr compared to those of ^{88}Sr and ^{90}Sr when $\theta=0°$. A comparison of spectra obtained with different θ's was used in order to check the absence of hyperfine components of ^{89}Sr under the signals from the even isotopes.

Displayed in Fig. 2 is the fluorescence spectrum of ^{89}Sr in the $^1S_0-{}^1P_1$ transition obtained at laser powers of 50 μW. The observed linewidth is 40 MHz at FWHM composed of the natural linewidth of 33 MHz (Ref. 11) and a residual Doppler width. Since the natural linewidth is dominant, a least squares analysis with pure Lorentzian line shapes is applied to the spectra obtained in the $\lambda=460$ nm line. For the least squares analysis of ^{87}Sr, the known hyperfine structure splitting of the $^1P_1$ state[12] was used in order to reduce the number of free fitting parameters. The spectra from the ^{89}Sr probe were fitted with five Lorentzians of identical linewidths. The IS between ^{88}Sr and ^{90}Sr was kept variable. The IS measured between these two isotopes reproduces very well the precisely measured value obtained in the ^{90}Sr sample where no ^{89}Sr was present. No attempt was made to identify the individual hyperfine structure components of ^{89}Sr, and the IS of this isotope is determined from the center of gravity of the observed signal. The quoted error for the IS describes the variation in the position of the center of gravity obtained from different sets of data which included spectra made up by summing up to 12 spectra. In the case of the $^1S_0$-$^3P_1$ transition, the spectra of the stable isotopes were fitted using pure Gaussians since the observed linewidth of 8 MHz is governed by the residual Doppler width [$\Delta\nu_{nat}=8(1)$ KHz].[11] The results obtained for the IS of the measured isotopes are given in Table I. Our values for the IS of the stable isotopes are in excellent agreement with the results published recently by other authors.[13,14] In the case of ^{90}Sr our more precise result disagrees slightly with an older measurement by Heilig [IS ^{90,88}Sr $=228(18)$ MHz].[15]

III. EVALUATION OF CHANGES IN MEAN SQUARE CHARGE RADII

Changes in mean square charge radii ($\delta\langle r^2\rangle^{AA'}$) between the investigated isotopes are obtained from the IS data following the standard procedure described by Heilig and Steudel.[1] The IS between two isotopes A and A' is the sum of the normal mass shift $\delta\nu_{NMS}^{AA'}$, the specific mass shift $\delta\nu_{SMS}^{AA'}$, and the field shift $\delta\nu_{FS}^{AA'}$.

$$IS^{AA'}=\nu^{A'}-\nu^{A}=\delta\nu_{NMS}^{AA'}+\delta\nu_{SMS}^{AA'}+\delta\nu_{FS}^{AA'} . \quad (1)$$

The $\delta\nu_{FS}^{AA'}$ is proportional to $\delta\langle r^2\rangle^{AA'}$, i.e.,

$$\delta\nu_{FS}^{AA'}=F\delta\langle r^2\rangle^{AA'} . \quad (2)$$

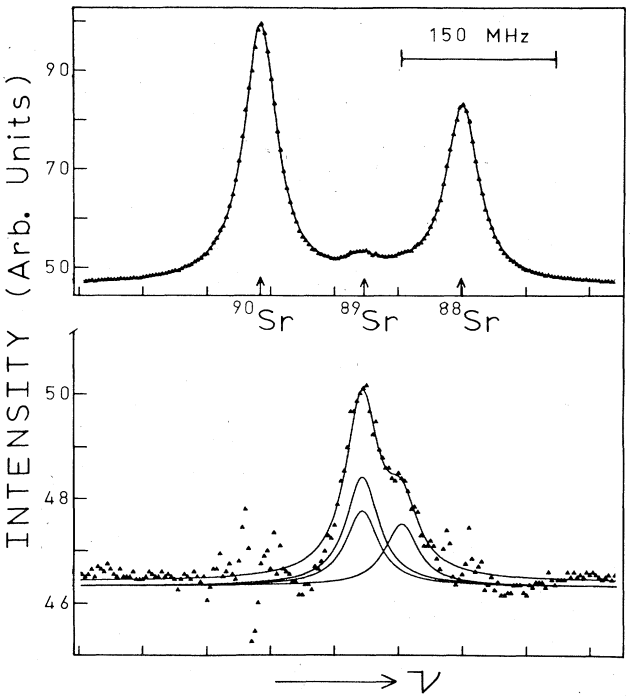

FIG. 2. Upper part: signal of ^{88}Sr, ^{89}Sr, and ^{90}Sr in the $5s^2\ {}^1S_0-5s\,5p\ {}^1P_1$ transition. The solid line represents a theoretical fit using five Lorentzians; the arrows indicate the centers of gravity. Lower part: expanded curve for the ^{89}Sr region, obtained by subtracting fits to the ^{88}Sr and ^{90}Sr peaks from the data. The solid lines show the overall fit as well as the three Lorentzians under the curve found from the fit.

Contributions of higher radial moments to the change in charge radius [2% in Sr (Ref. 16)] are neglected. In order to extract $\delta\langle r^2\rangle^{AA'}$ from the measured $IS^{AA'}$, then $\delta\nu_{NMS}^{AA'}$, $\delta\nu_{SMS}^{AA'}$, and the constant F have to be known. Whereas $\delta\nu_{NMS}^{AA'}$ can be easily calculated,[1] $\delta\nu_{SMS}^{AA'}$ and the calibration factor F are subject to various uncertainties which, however, can be minimized by comparing optical IS data with $\delta\langle r^2\rangle$ values obtained from mesic experiments. The calibration of $\delta\langle r^2\rangle$ from optical IS data in Sr has been discussed extensively by Bender *et al.* for various transitions.[14] From their work we obtain $\delta\nu_{SMS}^{AA'}=(-0.12\pm0.08)\delta\nu_{NMS}^{AA'}$, $F=(-896\pm130)$ MHz/fm^2 for the $^1S_0$-$^1P_1$ transition and $\delta\nu_{SMS}^{AA'}=(0.8\pm0.5)\delta\nu_{NMS}^{AA'}$, $F=(-1106\pm165)$ MHz/fm^2 for the $^1S_0$-$^3P_1$ transition. Using these values we derive from our IS data the $\delta\langle r^2\rangle$ values listed in the second column of Table II. For the stable isotopes we quote weighted mean values obtained

TABLE I. Measured isotope shifts in atomic strontium.

Transition	$\nu^{88}-\nu^{A}$ (MHz) $A=84$	$A=86$	$A=87$	$A=89$	$A=90$
$5s^2\ {}^1S_0\rightarrow 5s\,5p\ {}^1P_1$	270.6(2.4)	124.5(1.3)	49.2(3.6)	93.1(7.1)	206.2(2.4)
$5s^2\ {}^1S_0\rightarrow 5s\,5p\ {}^3P_1$	351.2(1.4)	164.0(0.8)	62.5(1.0)		

TABLE II. Experimental changes of mean square charge radii for the investigated isotopes relative to ^{88}Sr (second column). The quoted errors are due to experimental errors only. In the fourth column we give the predictions for the changes in mean square charge radii from the droplet model with the deformation parameter α_2^2 (calc) (third column) obtained from the calculated quadrupole moments in Ref. 19. The last column gives the droplet model predictions using the deformation parameter α_2^2 (expt) (fifth column) derived from experimental $BE2$ values as described in the text.

A	$\delta\langle r^2\rangle^{A,88}$ (expt) (fm^2)	α_2^2 (calc) (10^{-3})	$\delta\langle r^2\rangle_D^{A,88}$ (fm^2)	α_2^2 (expt) (10^{-3})	$\delta\langle r^2\rangle_D^{A,88}$ (fm^2)
90	−0.318(3)	0.65	−0.122	16.1(3.7)	−0.207
89	−0.147(8)	1.16	−0.073		
88	0	0.07	0	5.05(0.12)	0
87	−0.006(2)	1.18	0.040		
86	−0.047(2)	0.30	0.110	7.56(0.96)	0.075
84	−0.110(2)	0.30	0.223	10.5(1.8)	0.145

from the IS measurements in both lines. The errors given are experimental errors since the systematic errors in $\delta\nu_{SMS}^{AA'}$ and F affect only the absolute values of $\delta\langle r^2\rangle$ but not their overall trend. For an illustration of the influence of the uncertainty of $\delta\nu_{SMS}^{AA'}$ and F on $\delta\langle r^2\rangle$ we have plotted $\delta\langle r^2\rangle^{A,88}$ vs A in Fig. 3 and included in this figure the behavior of $\delta\langle r^2\rangle^{A,88}$ for values of $\delta\nu_{SMS}$ and F deviating by one error interval. In Fig. 4 we compare the changes of mean square charge radii in Sr with those of some neighboring elements of Kr,[5] Rb,[17] Zr,[1] and Mo.[18] The $\delta\langle r^2\rangle$'s of the Sr and its neighbors show a quite similar behavior over the mass range considered here. The charge radii decrease uniformly with increasing N and reach a minimum for $N=50$, where the shell closure is pronounced as a distinct kink in the $\delta\langle r^2\rangle$ data of Sr and Rb. A sharp increase of $\langle r^2\rangle$ is observed for the neutron-rich isotopes in Rb, Sr, Zr, and Mo.

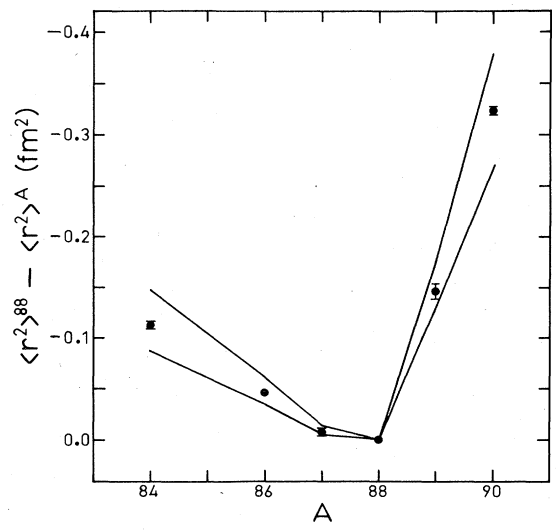

FIG. 3. Changes of mean square charge radii of Sr derived from the isotope shift measurements in the $\lambda=460.7$ nm line. The solid lines correspond to the values of $\langle r^2\rangle^{88}-\langle r^2\rangle^A$ when the specific mass shift and the calibration factor F are altered by one error interval (upper line: $\delta\nu_{SMS}^{AA'}=-0.2\delta\nu_{NMS}^{AA'}$, $F=-766$ MHz/fm^2; lower line: $\delta\nu_{SMS}^{AA'}=-0.04\delta\nu_{NMS}^{AA'}$, $F=-1026$ MHz/fm^2).

IV. DISCUSSION

A. Comparison with the droplet model predictions

The changes in mean square charge radii for the Sr isotopes can be compared to the predictions from the droplet model.[3] In this model, the mean square charge radius of an isotope A ($\langle r^2\rangle^A$) is calculated from contributions of the size and shape of the nucleus ($\langle r^2\rangle_u^A$), the internal redistribution of the charge induced by Coulomb repulsion ($\langle r^2\rangle_r^A$), and the diffuseness of the nuclear surface ($\langle r^2\rangle_d^A$). For calculating changes in mean square charge radii we have used

$$\delta\langle r^2\rangle^{AA'}=\langle r^2\rangle^{A'}-\langle r^2\rangle^A \tag{3}$$

with

$$\langle r^2\rangle^A=\langle r^2\rangle_u^A+\langle r^2\rangle_r^A+\langle r^2\rangle_d^A \tag{4}$$

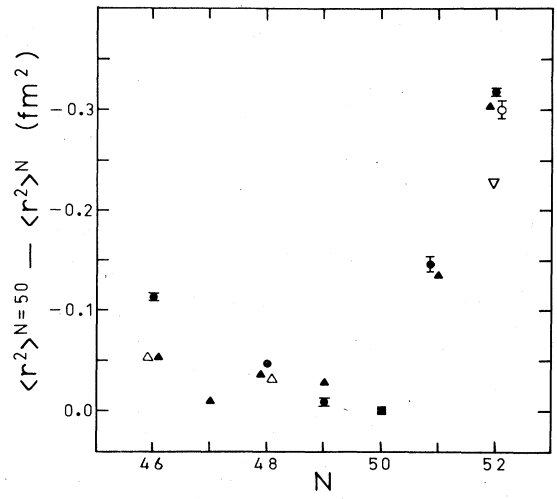

FIG. 4. Changes of mean square charge radii of Sr (solid circles) (this work), Rb (solid triangles) (Ref. 17), Kr (open triangles) (Ref. 5), Zr (open circle) (Ref. 1), and Mo (open inverted triangle) (Ref. 18) near the $N=50$ shell closure.

and

$$\langle r^2\rangle_u^A=\tfrac{3}{5}R^2(1+\alpha_2^2)\,, \tag{5}$$

$$\langle r^2\rangle_r^A=\tfrac{12}{175}C'R^2(1+\tfrac{14}{5}\alpha_2^2)\,, \tag{6}$$

$$\langle r^2\rangle_d^A=3b^2\,. \tag{7}$$

The "deformation-dependent radius" R, the deformation parameter α_2^2, the A- and Z-dependent constant C', and the surface width b are defined in Ref. 3. For calculating $\langle r^2\rangle^A$ we have neglected terms of order higher than α_2^2 and contributions to the nuclear shape from hexadecapole moments. The parameter α_2 can be obtained from the calculated ground state electric quadrupole moments (Q_2) tabulated by Möller and Nix[19] using the relation[3]

$$Q_2=\tfrac{6}{5}ZR^2\alpha_2(1+\tfrac{8}{35}C')\,. \tag{8}$$

We have compiled in the third column of Table II the calculated deformation parameters (α_2^2 calc) and listed in the fourth column of this table the resulting droplet values for $\delta\langle r^2\rangle^{A,88}$. It should be noted that the surface width b has no A or Z dependence and that the $\delta\langle r^2\rangle^{AA'}$ values are unaffected by this term.

A comparison of the predictions from the droplet model with the experimental changes in mean square charge radii shows that the agreement is poor. An increase in charge radii is predicted over the complete mass sequence, but only observed for isotopes with $N>50$. The disagreement between model prediction and experimental changes in mean square charge radii might be due to an underestimation of the nuclear deformation obtained from the calculated quadrupole moments from which only the static contribution to the deformation is derived. The Sr nuclei considered here, however, are known to have a pronounced vibrational character, which suggests that their deformation arises from dynamic as well as from static contributions.

Deformation parameters, which include both static and dynamic contributions to the nuclear deformation, can be derived for the even-even isotopes ^{84,86,88}Sr from the reduced transition probabilities for $E2$ transitions using[20]

$$B(E2\ 0^+\rightarrow 2^+)=\left[\frac{3}{4\pi}Ze(1.2A^{1/3})^2\right]^2\beta^2\,. \tag{9}$$

Although this relation was derived for strongly deformed rotational nuclei, it was pointed out by Kumar[21] that it is valid for even-even nuclei in a model-independent way. For the light elements, the term is connected to α_2^2, to a good approximation, by

$$\alpha_2^2=\frac{5}{4\pi}\beta^2\,. \tag{10}$$

For ^{90}Sr where no $BE2$ values are measured, the reduced transition probability can only be roughly estimated from the energy of the first excited 2^+ level (E_{2^+}) using the general empirical rule

$$B(E2\ 0^+\rightarrow 2^+)E_{2^+}=(12\pm4)10^{-3}Z^2A^{-1}\ (\mathrm{MeV}\,e^2\mathrm{b}^2)\,, \tag{11}$$

which, as shown by Grodzins,[22] holds for the first excited 2^+ states of even-even nuclei almost throughout the nuclear chart. The parameter β derived from $BE2$ values[23–26] is plotted as a function of the neutron number in Fig. 5. The weighted mean values for α_2^2 (expt) obtained from β^2 are listed in the fifth column of Table II. Calculated and experimental deformation parameters indicate a decrease in nuclear deformation when the closed neutron shell at $N=50$ is approached. The observed discrepancy in the absolute values of α_2^2 (expt) and α_2^2 (calc) supports the argument of a dominant dynamic contribution to the nuclear deformation.

We use α_2^2 (expt) instead of α_2^2 (calc) in order to calculate a new set of droplet predictions for the changes in mean square charge radii of even-even Sr isotopes. These calculated values are included in Table II. Whereas for the change in mean square charge radius between ^{88}Sr and ^{90}Sr a quantitative comparison between calculated and experimental values is somewhat handicapped by the rough estimate of the deformation of ^{90}Sr, for the neutron-deficient isotopes the trend of decreasing charge radii with increasing neutron number remains unexplained.

A similar disagreement between changes in mean square charge radii obtained from IS measurements of Kr isotopes below the $N=50$ shell closure and those calculated from the two-parameter model with the inclusion of deformations derived from $BE2$ values has been stated by Gerhardt *et al.*[5] In their discussion, the authors suggest the expansion of the two-parameter model by a third term describing the change of the skin thickness of the nuclear charge distribution.

Following these lines also for the case of Sr, we allow a variation of the surface width b with mass number in the droplet expression for $\langle r^2\rangle^A$ [Eq. (4)]. We use $b=0.908$ fm for ^{88}Sr from electron scattering experiments[27] (e.g., $\delta^{(1)}$ in Table 3 of Ref. 27, corrected for quadrupole deformation with the help of $BE2$ values) and α_2^2 (expt) from above and we calculate the surface widths of the remaining even isotopes in order to reproduce the experimental

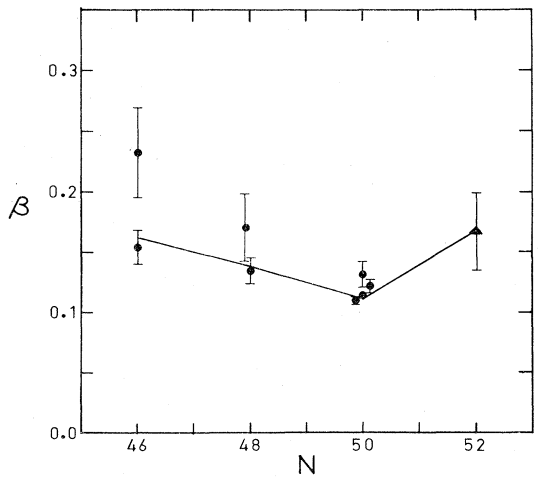

FIG. 5. Deformation parameters β of the Sr isotopes derived from $BE2$ values (circles) and the energy of the first excited 2^+ state (triangle) (Refs. 22–26). The solid line connects the weighted mean values which are used in the discussion of the changes in mean square charge radii.

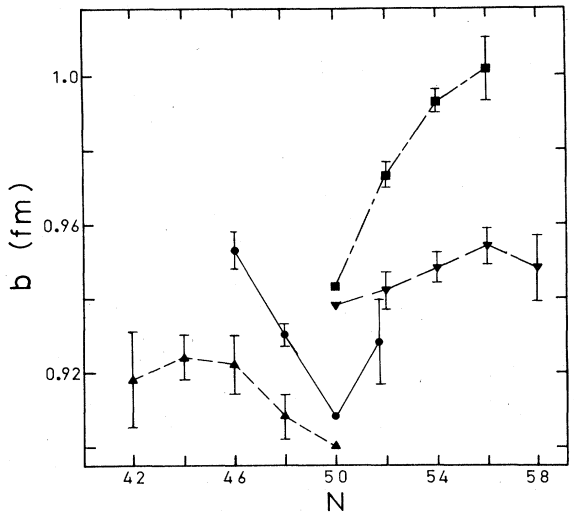

FIG. 6. Surface widths b extracted from experimental changes in mean square charge radii of Sr (circles) (this work), Kr (triangles) (Ref. 5), Zr (squares) (Ref. 1), and Mo (inverted triangles) (Ref. 18). The errors given are due to the uncertainties in the experimental IS measurements and $BE2$ values, which are used in order to correct the droplet model prediction for quadrupole deformation (static and dynamic). (For the $BE2$ values for Kr see Ref. 5 and references therein, for Mo and Zr see Ref. 38. In calculating b for the different isotopes we have used b (corrected for quadrupole deformation) of ^{88}Sr, ^{90}Sr, and ^{92}Mo from Ref. 27. For ^{86}Kr, b has been arbitrarily chosen as $b=0.9$ fm.

changes in mean square charge radii. The values of b obtained in this way are plotted as a function of N in Fig. 6. It can be seen that it is possible to reproduce the experimental changes in mean square charge radii with changes in b of only a few percent. In Fig. 6 we have added the values of b for the Sr neighbors Kr, Zr, and Mo. The parameter b was calculated in the same way as in the Sr case from experimental changes in the mean square charge radii [Kr (Ref. 5), Zr (Ref. 1), Mo (Ref. 18)]. It can be seen that the general trend observed in strontium is well reflected in the neighboring elements: b decreases when the closed shell at $N=50$ is approached from the low as well as the high mass side. Skin thicknesses obtained from electron scattering data support the conclusion of a minimum in b at $N=50$. In Fig. 7 we have plotted the parameter b for Zr and Mo obtained from a compilation in Ref. 27 (again the contribution to b from the quadrupole deformation was subtracted with the help of $BE2$ values). The values for b extracted from IS measurements and electron scattering give the same consistent picture of small changes in the surface width near the closed shell with a minimum at $N=50$.

The effect of a nonconstant surface width in the charge distribution of the investigated Sr isotopes is also indicated by HF calculations, as will be shown in the following.

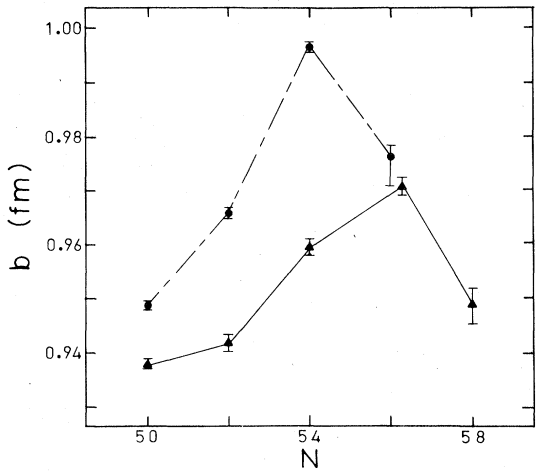

FIG. 7. Surface widths b from electron scattering data (Ref. 27) for Mo (triangles) and Zr (circles). The error bars are due to the uncertainties in the $BE2$ values used to correct the experimental values of b for contributions from quadrupole deformation.

B. HF calculations

1. *Comparison with the experimental data*

We have calculated the mean square radii (MSR) for protons ($\langle r_p^2 \rangle$) and charge ($\langle r_c^2 \rangle$) of the investigated even Sr isotopes in the framework of the spherical (constrained) HF plus BCS model using the effective force SKa (Ref. 8) and the finite range interaction G0P (Ref. 9).

The values for $\langle r_p^2 \rangle$ are listed in Table III, the sixth column. The corresponding values of $\langle r_c^2 \rangle$ were obtained by adding to $\langle r_p^2 \rangle$ the following corrections: the proton and the neutron form factors and the electromagnetic spin orbit interaction.[28,29] These corrections—as well as the correction for the spurious c.m. motion—were calculated as in Ref. 30. Among them the spin-orbit correction plays an interesting role because it is sensitive to the occupation of spin nonsaturated orbitals.[28] Because the BCS occupations[31]

$$V_j^2=\frac{2j+1}{2}\left[1-\frac{\epsilon_j-\lambda}{E_j}\right], \tag{12}$$

with

$$E_j=\begin{cases}(\epsilon_j-\lambda)^2+\Delta^2 \text{ active orbitals,}\\ \epsilon_j-\lambda \text{ nonactive orbitals}\end{cases}$$

in the BCS calculation are slightly different for the forces SKa and G0P when we use the same pairing strength in our calculations, we find slightly different contributions to the predicted $\langle r_c^2 \rangle$ with force SKa than with force G0P when we include the spin-orbit correction. The consequence is a small difference in the changes in MSR going from the change in proton MSR ($\delta\langle r_p^2 \rangle$) to changes in mean square charge radii ($\delta\langle r_c^2 \rangle$).

The values of $\delta\langle r_p^2 \rangle$) and $\delta\langle r_c^2 \rangle$ are compiled in Table IV, seventh and eleventh columns, and $\delta\langle r_c^2 \rangle$ is plotted in

TABLE III. Summary of the HF plus BCS calculations with forces SKa and G0P (first column) for the Sr series (second column). The binding energies per nucleon (third column) and the proton and neutron pairing gaps are included in the fourth and fifth columns. Proton and charge mean square radii are given in the sixth and ninth columns. The corresponding central radii C and surface width b are given in the seventh and tenth and the eighth and eleventh columns, respectively.

					Protons			Charge		
Force	Nucleus	E/A (MeV)	Δ_p (MeV)	Δ_n (MeV)	MSR (fm^2)	C (fm)	b (fm)	MSR (fm^2)	C (fm)	b (fm)
SKa	^{84}Sr	−8.632	0.848	1.253	17.3056	4.8302	0.8990	17.6677	4.7942	0.9737
	^{86}Sr	−8.682	0.797	1.144	17.3739	4.8442	0.8941	17.7140	4.8091	0.9661
	^{88}Sr	−8.716	0.752		17.4381	4.8582	0.8888	17.7553	4.8230	0.9585
	^{90}Sr	−8.665	0.770	1.138	17.5804	4.8727	0.8956	17.8878	4.8455	0.9612
G0P	^{84}Sr	−8.442	0.673	1.453	17.6324	4.8277	0.9124	17.9929	4.8176	0.9775
	^{86}Sr	−8.486	0.588	1.143	17.6694	4.8428	0.9032	18.0081	4.8329	0.9664
	^{88}Sr	−8.519	0.519		17.6862	4.8543	0.8941	18.0022	4.8436	0.9555
	^{90}Sr	−8.508	0.579	1.172	17.8143	4.8779	0.8965	18.1229	4.8711	0.9560

Fig. 8 for comparison with the experimental data and the predictions from the droplet model.

The predictions of the HF calculations, in comparison to the spherical droplet model in the standard parametrization of Ref. 3, represent an improvement of between 42% and 64% for $\delta\langle r_c^2\rangle^{86,88}$ and $\delta\langle r_c^2\rangle^{84,88}$, respectively, and a slight improvement for $\delta\langle r^2\rangle^{90,88}$. Whereas the droplet model predicts a uniform increase of the charge radii with increasing neutron number across the closed neutron shell at $N=50$, the shell closure is expressed in the HF calculations as a distinct kink in the curve of $\delta\langle r^2\rangle^{A,88}$.

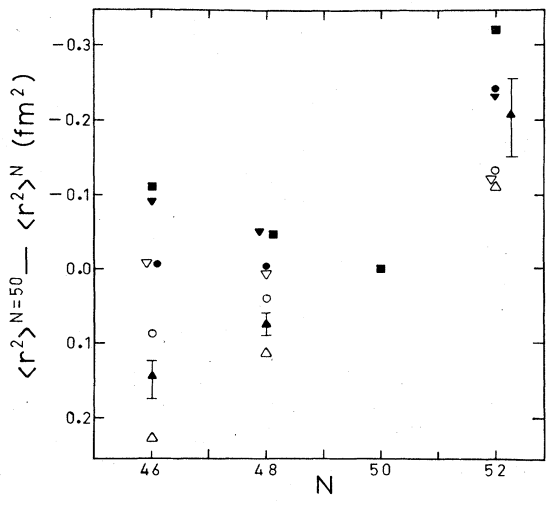

FIG. 8. Comparison of the experimental changes in mean square charge radii in Sr (squares) with predictions from the droplet model and HF plus BCS calculations: open triangles—spherical droplet model; open circles—HF plus BCS force SKa; open inverted triangles—HF plus BCS force G0P. The predictions corrected for changes in static and dynamic deformations (see the text) are indicated by the corresponding filled symbols. The errors arising from the uncertainty of the $BE2$ values used for the correction are indicated only for the droplet model prediction.

For a quantitative comparison between HF predictions and experimental data we have to consider the influence of changes in dynamic deformation between the investigated isotopes, which are not accounted for in the static HF calculations and which, as pointed out previously, lead to an important contribution to the changes in mean square charge radii. The effects of the zero point quadrupole motion can be roughly included by[32]

$$\langle \tilde{r}_c^2\rangle = \langle r_c^2\rangle[1+\alpha_2^2(\text{expt})-\alpha_2^2(\text{HF})]\ , \tag{13}$$

where α_2^2 (expt) is defined in Sec. IV A and α_2^2 (HF) is the deformation parameter from HF calculations. No significant effects of the static deformation on $\delta\langle r_c^2\rangle$ were found in our analysis performed using force G0P, and hence α_2^2 (HF) is neglected. Using α_2^2 (expt) compiled in Table II for the different isotopes, we calculate a new set of changes in mean square charge radii ($\delta\langle \tilde{r}_c^2\rangle$) for the even Sr isotopes. The results are included in Fig. 8.

The values indicate, for both forces, a decrease in the mean square charge radius with increasing N for the isotopes with $N<50$. The agreement of $\delta\langle \tilde{r}_c^2\rangle$ with the experiment over this mass range is excellent for force G0P, considering the uncertainty in the $BE2$ values used for correcting the predictions for quadrupole deformations and the accuracy with which $\delta\langle r^2\rangle^{AA'}$ can be derived from the IS measurements (see Fig. 3). Within these limits of errors, the HF predictions from forces SKa and G0P agree well with the experimental data for the case $\delta\langle r^2\rangle^{90,88}$.

2. *Leptodermous interpretation of the HF plus BCS calculations*

In the following subsection we shall focus our attention on changes of the surface thickness in the series of Sr isotopes and give a leptodermous interpretation of the HF plus BCS model.

By definition the mean square radius [$q=p$ (protons), $q=c$ (charge)]

TABLE IV. Changes in mean square radii for protons and charge, using the interactions SKa and G0P, for the investigated Sr isotopes (second column). The droplet model values [parameters of the force SKa (Ref. 39)], obtained as in Ref. 7, are given in the third column. The fourth, fifth, eighth, and ninth columns give the predictions of the leptodermous two-parameter model of Eq. (18) when (a) only isotopic changes in C are considered and the surface width b is kept constant at $\bar{b}=\frac{1}{4}\sum_{A=84}^{90} b(A)$, A=even (the fourth and eighth columns) and (b) both C and b are varied (the fifth and ninth columns). In the sixth and tenth columns we give $\delta\langle r^2\rangle^{A,88}$ calculated using the symmetrized proton and charge densities [Eq. (16)]. The HF results are given in the seventh and eleventh columns.

			$\delta\langle r^2\rangle^{A,88}$ (fm^2) HF plus BCS							
			Protons				Charge			
			Leptodermous		Symm	HF	Leptodermous		Symm	HF
Force	A	DM	(a)	(b)			(a)	(b)		
SKa	84	0.314	0.160	0.075	0.082	0.132	0.162	0.022	0.041	0.087
	86	0.157	0.080	0.036	0.041	0.064	0.078	0.009	0.018	0.041
	88	0	0	0	0	0	0	0	0	0
	90	−0.157	−0.083	−0.140	−0.132	−0.142	−0.128	−0.153	−0.147	−0.132
G0P	84		0.152	−0.003	0.016	0.054	0.148	−0.055	−0.025	−0.009
	86		0.069	−0.011	−0.001	0.017	0.061	−0.038	−0.008	0.006
	88		0	0	0	0	0	0	0	0
	90		−0.135	−0.156	−0.154	−0.128	−0.157	−0.162	−0.157	−0.121

$$\langle r_q^2\rangle = 4\pi \int_0^\infty \rho_q(r) r^4 dr / Z \tag{14}$$

[where

$$Z = 4\pi \int_0^\infty \rho_q(r) r^2 dr$$

is the charge of the nucleus] is most sensitive to the external region of the charge density. We exploit this property of the MSR to interpret its value as a function of the following two leptodermous parameters:[33,34]

(a) C_q defined as the distance from the center of the nucleus to the point at the surface where the slope of the density is at a maximum;

(b) b_q defined as the symmetrical surface width.

$$b_q = \left[\frac{\int_{c_q}^\infty \rho_q'(r)(r-C_q)^2 dr}{\int_{c_q}^\infty \rho_q'(r) dr} \right]^{1/2} . \tag{15}$$

This definition of b_q is equivalent to replacing the actual density $\rho_q(r)$ by

$$\begin{aligned} \rho_q(r)^{\text{symm}} &= \rho_q(r) \quad \text{for } r \geq C_q \\ &= 2\rho_q(C_q) - \rho_q(2C_q - r) \quad \text{for } r < C_q . \end{aligned} \tag{16}$$

In this approximation we neglect the following contributions to the MSR: (a) the asymmetry and (b) the shell effects in the core region for a distance $r \lesssim C_q - 0.9$ fm from the center of the nucleus.[33–35]

Note that our leptodermous interpretation is model independent in the sense that no arbitrary function was fitted to the analyzed HF plus BCS densities.[33] The parameter b_q is connected to the surface parameter b used in Sec. IV A by

$$b_q \propto b \frac{t_d}{t_H} , \tag{17}$$

with $t_H = 2.54b$, $t_d = 1.098\rho_{\text{bulk}}/\rho'_{\max}$, and $t_H/t_d = \text{const} \cong 0.963$ fm in the mass region $88 < A < 100$ as shown in Fig. 6(b) of Ref. 27.

Table III contains the leptodermous parameters C_q and b_q corresponding to the proton and charge densities predicted by the HF plus BCS model.[36,33,30] Both forces predict an increase in C_q with increasing neutron number and a change of the surface width b_q. The surface width has a minimum for ^{88}Sr with the magic neutron number $N=50$. This behavior of the surface thickness is consistent with the picture obtained before in the comparison of the experimental isotope shift data to the droplet model.

At this point we should stress that still other effects may have a significant influence on the value of $\delta\langle r_q^2\rangle^{AA'}$, as can be seen in Table IV. There we find that the values of $\delta\langle r_q^2\rangle^{A,88}$ (see the sixth and tenth columns) using Eq. (16) for $\rho_q(r)$ are closer to the HF values $\delta\langle r^2\rangle^{A,88}$ (see the seventh and eleventh columns) than those using the simpler leptodermous approximation:[37]

$$\langle r_q^2\rangle = \tfrac{3}{5} C_q^2 \left[1 + \frac{7}{2} \frac{b_q^2}{C_q^2} \right]^2 \tag{18}$$

(see the fifth and ninth columns). The remaining discrepancies have to be attributed to "higher order effects" such as changes (i) in the asymmetry and (ii) in the oscillations of the actual density in the nuclear core region, in going from one isotope to another, effects which are not included in our symmetrized $\rho_q(r)$ [Eq. (16)].

V. SUMMARY AND CONCLUSION

Isotope shifts in the stable Sr isotopes and the radioactive isotopes ^{89}Sr and ^{90}Sr were measured by laser spec-

troscopy on collimated atomic beams. The changes in mean square charge radii extracted from these measurements show a decrease when the closed neutron shell at $N=50$ (^{88}Sr) is approached from the neutron-deficient as well as the neutron-rich side. A comparison of the experimental data with predictions from the droplet model and HF plus BCS calculations indicates that the changes in mean square charge radii are due to a change in size, a change in (predominantly dynamic) deformation, and a change in the surface width of the nuclear charge distribution. The observed changes in surface thickness are on the order of 1—2 % between neighboring even isotopes. The systematics, as well as the magnitude of the surface changes, are consistent with those derived from IS measurements of Kr, Zr, and Mo and those obtained from electron scattering data of Zr and Mo near the $N=50$ shell closure. The strong influence of even small changes in the diffuseness on the changes in mean square charge radii suggest that it is by no means straightforward to extract changes in nuclear deformation from the difference between predictions of the droplet model and experimental changes in mean square charge radii. One also has to consider the changes in diffuseness in more detail. For this purpose, calculations in a microscopic model, e.g., HF plus BCS calculations, are a valuable help.

ACKNOWLEDGMENTS

We would like to thank Dr. S. Büttgenbach for his participation in parts of the experiment and for stimulating discussions. This work was supported at McGill by the Natural Sciences and Engineering Research Council (Canada) and at McMaster by NSERC under Grant A-3198.

[1]K. Heilig and A. Steudel, At. Data Nucl. Data Tables **14**, 613 (1974).
[2]S. Ulrich and E. W. Otten, Nucl. Phys. **A248**, 173 (1975).
[3]W. D. Myers and K. H. Schmidt, Nucl. Phys. **A410**, 61 (1983).
[4]E. W. Otten, Nucl. Phys. **A354**, 471 (1981).
[5]H. Gerhardt, E. Matthias, H. Rinneberg, F. Schneider, A. Timmerman, R. Wenz, and P. J. West, Z. Phys. A **292**, 7 (1979).
[6]R. Wenz, A. Timmerman, and E. Matthias, Z. Phys. A **303**, 87 (1981).
[7]D. Berdichevsky and F. Tondeur, Z. Phys. A **322**, 141 (1985).
[8]H. S. Köhler, Nucl. Phys. **A258**, 301 (1976).
[9]M. N. Butler, D. W. L. Sprung, and J. Martorell, Nucl. Phys. **A422**, 157 (1984).
[10]G. H. Fuller, J. Phys. Chem. Ref. Data **5**, 835 (1976).
[11]M. W. Swagel and A. Lurio, Phys. Rev. **169**, 114 (1968).
[12]H. J. Kluge and H. Sauter, Z. Phys. **270**, 295 (1974).
[13]E. R. Eliel, W. Hogervorst, T. Olsson, and L. R. Pendrill, Z. Phys. A **311**, 1 (1983).
[14]D. Bender, H. Brand, and V. Pfeufer, Z. Phys. A **318**, 291 (1984).
[15]K. Heilig, Z. Phys. **161**, 252 (1961).
[16]E. C. Seltzer, Phys. Rev. **188**, 1919 (1969).
[17]C. Thibault, F. Touchard, S. Büttgenbach, R. Klapisch, M. de Saint Simon, H. T. Duong, P. Jacquinot, P. Juncar, S. Liberman, P. Pillet, J. Pinard, J. L. Vialle, A. Pesnelle, and G. Huber, Phys. Rev. C **23**, 2720 (1981).
[18]P. Aufmuth, H. D. Clieves, K. Heilig, A. Steudel, D. Wendlandt, and F. Bauche, Z. Phys. A **285**, 357 (1978).
[19]P. Möller and J. R. Nix, At. Data Nucl. Data Tables **26**, 165 (1981).
[20]P. H. Stelson and L. Grodzins, Nucl. Data Tables **A1**, 21 (1965).
[21]K. Kumar, Phys. Rev. Lett. **28**, 249 (1972).
[22]L. Grodzins, Phys. Lett. **2**, No. 2, 88 (1962).
[23]H. W. Müller and J. W. Tepel, Nucl. Data Sheets **27**, No. 3, 339 (1979).
[24]J. W. Tepel, Nucl. Data Sheets **25**, No. 4, 553 (1978).
[25]R. L. Bunting and J. J. Kraushaar, Nucl. Data Sheets **18**, No. 2, 87 (1976).
[26]*Table of Isotopes*, 7th ed., edited by C. M. Lederer and V. S. Shirley (Wiley, New York, 1978).
[27]J. Friedrich and N. Voegler, Nucl. Phys. **A373**, 192 (1982).
[28]W. Bertozzi, J. L. Friar, J. Heisenberg, and J. W. Negele, Phys. Lett. **41B**, 408 (1972).
[29]H. Chandra and G. Sauer, Phys. Rev. C **13**, 245 (1976).
[30]X. Campi, D. W. L. Sprung, and J. Martorell, Nucl. Phys. **A223**, 541 (1974).
[31]S. T. Beliaev, K. Dan Vidensk. Selsk. Mat. Fys. Medd. **31**, No. 11 (1959).
[32]R. A. Uher and R. A. Sorensen, Nucl. Phys. **86**, 1 (1966).
[33]D. Berdichevsky and U. Mosel, Nucl. Phys. **A388**, 205 (1982).
[34]D. Berdichevsky, J. Phys. C **6**, 221 (1984).
[35]D. Berdichevsky, Ph.D. thesis, University of Giessen, 1982.
[36]J. L. Friar and J. W. Negele, Adv. Nucl. Phys. **8**, 219 (1975).
[37]G. Süssman, Z. Phys. A **274**, 145 (1975).
[38]P. M. Endt, At. Data Nucl. Data Tables **26**, No. 1, 47 (1981).
[39]F. Tondeur and D. Berdichevsky submitted to Z. Phys.